Touchless Multiview Fingerprint Acquisition and Mosaicking

Feng Liu, David Zhang, *Fellow, IEEE,* Changjiang Song, and Guangming Lu

***Abstract*—Touchless fingerprint capture devices have the advantage over traditional touch-based approaches of being hygienic and preventing distortions resulting from the contact of fingers. Single-view acquisition systems bring in problems, such as scene difference and a limited effective area. This paper thus presents a touchless multiview fingerprint capture system that acquires three different views of fingerprint images at the same time. This device is designed by optimizing parameters regarding the captured fingerprint image quality and device size. A fingerprint mosaicking method is proposed to splice together the captured images of a finger to form a new image with a larger useful print area. Optimization design of our device is demonstrated by introducing our design procedure and comparing with current touchless multiview fingerprint acquisition devices. The efficiency of our device is further proved by comparing recognition accuracy between mosaicked images and touch-based fingerprint images. Experimental results also show that our proposed mosaicking method is more robust to low ridge–valley contrast fingerprint images than available methods. The effectiveness of our mosaicking method is further proved by comparing equal error rates with the mosaicking algorithms evaluated on our established database of 541 fingers.**

***Index Terms*—Device design, fingerprint acquisition, fingerprint mosaicking, RANdom SAmple Consensus, scale invariant feature transformation, touchless multiview imaging**

I. Introduction

FINGERPRINTS have been used for personal identification for centuries and automatic fingerprint identification systems have been used for decades. Nowadays fingerprint technique has been widely used in both forensic and civilian applications. Compared with other biometric features, fingerprint-based biometric is the most proven technique and has the largest market shares. Although fingerprint recognition has been studied for many years and much progress has been made, the performance of state-of-the-art matchers is still much lower than the expectations of people and theory estimation [1]. Until now, processing low-quality latent prints has still needed human intervention. In addition to the requirement for higher accuracy and speed, many new requirements have also risen along with increasing adoption of fingerprint technique in civilian applications, such as template security, hygiene, and so on. Fingerprint images can be acquired in off-line or online mode. The so-called ink-technique and extraction of latent fingerprints in crime scenes are examples of offline acquisition. Nowadays online acquisition techniques have been widely used. Common online acquisition techniques include optical, solid-state, thermal, and ultrasound [2]. Optical devices work in either touch-based or touchless mode. Frustrated total internal reflection (FTIR), as a well-known touch-based fingerprint imaging technique, is used in most of government and forensic applications due to its excellent image quality and low cost. Touchless optical fingerprint imaging is actually not a novel technique. It uses cameras to directly image the fingertip. It has the advantages of hygiene, no latent prints, and no distortion caused by pressure. As its image quality is lower than that of FTIR images and its size is bigger than that of solid-state sensors, this type of fingerprint device is currently seldom found in the market. However, in recent years, with emergence of more applications, popularity of multimodal biometrics, and development of fingerprint algorithms, there is necessity of reconsidering touchless fingerprint imaging technique. Earlier works about touchless fingerprint imaging devices began from single-camera mode [3]–[8]. Song *et al.* [3] designed a touchless fingerprint device using a monochrome CCD camera and double ring-type illuminators with blue LEDs. They stated that good quality images can be obtained by using the ring-type illuminators and some algorithmic amendments. Products of touchless fingerprint sensors from companies (e.g., Mitsubishi [4], TST Biometrics [5], and Lumidigm [6]) are on sale. Chen [7] described a device that captures 3-D shape of finger by using structured lights with one camera and one projector. Kumar and Zhou [8] used a simple web camera to capture very low resolution fingerprint images. These kinds of devices all face the problem of view difference due to curvature of the finger shape. In real fingerprint recognition systems, the performance is degraded by the limited common area between fingerprints caused by view difference. To deal with the above-mentioned problem, multiview touchless sensing techniques have been proposed [9]–13]. Typically, TBS [11] proposed a

Manuscript received August 28, 2012; revised December 17, 2012; accepted December 18, 2012. Date of publication July 17, 2013; date of current version August 7, 2013. This paper was supported in part by the GRF Fund from the HKSAR Government, the Central Fund from Hong Kong Polytechnic University, the NSFC Fund under Grants 61020106004, 61272292, and 61271344, the Shenzhen Fundamental Research Fund (JC201005260184A), and the Key Laboratory of Network Oriented Intelligent Computation, Shenzhen, China. The Associate Editor coordinating the review process was Dr. S. Shirmohammadi.

F. Liu and D. Zhang are with the Biometrics Research Center, Department of Computing, The Hong Kong Polytechnic University, Kowloon, Hong Kong (e-mail: csdzhang@comp.polyu.edu.hk).

G. Lu is with the Biocomputing Research Laboratory, Shenzhen Graduate School, Harbin Institute of Technology, Shenzhen, China.

C. Song is with the Institute of Automation, Heilongjiang Academy of Sciences, Harbin, China.

Color versions of one or more of the figures in this paper are available online at http://ieeexplore.ieee.org.

Digital Object Identifier 10.1109/TIM.2013.2258248

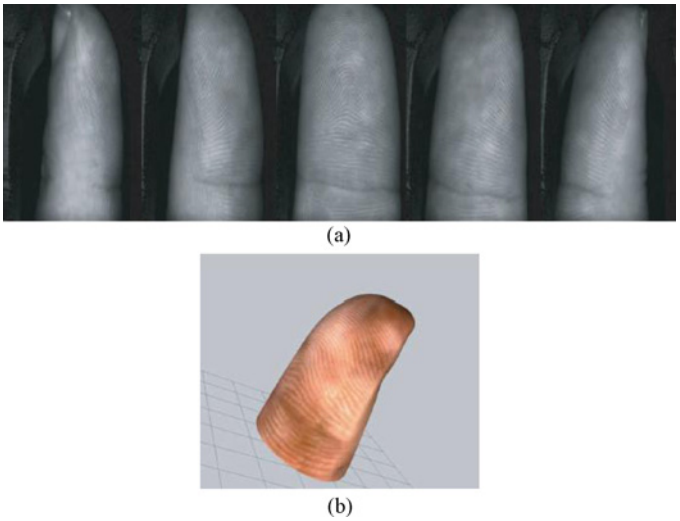

Fig. 1. Example images [14]. (a) Different views of fingerprint images captured by Surround Imager^{TM}. (b) Reconstructed 3-D finger shape.

3-D multicamera touchless fingerprint device named Surround Imager™ by using five cameras to capture nail-to-nail fingerprint images at one time and provided the reconstructed 3-D finger shape, as shown in Fig. 1 [14]. In this paper, they gave a brief description of the device design and related algorithms about 3-D reconstruction and recognition. However, the detail of algorithms have not been given and performance evaluation has not been reported. Later, they continued to improve their device and developed new versions of products by using three cameras at one time [12]. The detail specifications of the devices and algorithms for image processing are yet not available. Choi *et al.* [13] suggested using a single camera and two planar mirrors to form the multiview fingerprint imaging device. The side views of the finger reflected by these mirrors are captured by the central camera to form multiviews of fingerprint images. This device has the advantage of low cost, but the hardware design is very complex. For instance, the depth of field (DOF) of the central camera should be large enough to cover the three views of finger with high clarity. The setting of mirror and finger should be carefully considered due to the different size of finger. Such system has two difficulties: i) dividing the whole image (Fig. 2) into three segments manually. Constant threshold is not suitable to different size of fingers, as shown in Fig. 2; and ii) Stereo calibration for 3-D reconstruction. Current techniques for stereo calibration are mostly based on separate pictures captured by different cameras. The effective area in side-view images provided by mirror-reflected device is normally smaller than the one offered by multicamera-based device [see Figs. 1(a) and 2]. Table I summarizes the strengths and weaknesses of these two typical touchless multiview fingerprint imaging systems.

Due to the drawbacks of the mirror-reflected imaging technique, multicamera mode is adopted in this paper to design our fingerprint acquisition device. Meanwhile, considering the drawbacks and difficulties to get detail specifications of existing multicamera mode devices, as well as the unavailability

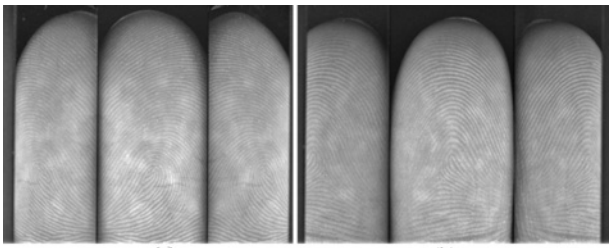

Fig. 2. Fingerprint images of two different fingers captured by the mirror-reflected device [13].

TABLE I
COMPARISON OF STRENGTHS AND WEAKNESSES OF TWO TYPICAL TOUCHLESS MULTIVIEW FINGERPRINT IMAGING DEVICES

Device	Strengths	Weaknesses
Surround Imager^{TM}	Cover larger effective area and possible to achieve 3-D reconstruction	Relatively expensive,
Mirror-reflected imaging device	Low cost	High hardware designing complexity, manually segmentation of region of interest (ROI) and, limited effective area in side-view images reflected by mirrors

of large-scale touchless multiview fingerprint databases in the public domain, this paper designed a touchless multiview fingerprint capture device using multicamera mode with optimized device parameters. Both image quality and device size are considered in designing the capture device. We established a database with 541 fingers. Based on the established database, the mosaicking technique is studied. For mosaicking, we firstly extract the scale invariant feature transformation (SIFT) features on each image, followed by matching them using RANdom SAmple Consensus (RANSAC) algorithm to estimate the transformation model, then extract the stitching line by comparing the similarity of overlapping region, and, finally, generate the mosaic image after Gaussian smoothing. The rest of the paper is organized as follows. In Section II, the detail of the touchless multiview fingerprint acquisition device are presented. In Section III, a fingerprint image mosaicking algorithm is proposed for stitching the multiple fingerprint images captured from different views into one single fingerprint image. Performance analysis and comparison is given in Section IV. Section V concludes the paper and suggests the future directions.

II. FINGERPRINT ACQUISITION

With the motivation of designing a cheaper and more optimized touchless multiview fingerprint capture device, we studied and selected the system parameters in this section. The schematic diagram of the device is shown in Fig. 3. Cameras are focused on the finger. LEDs are used to light the finger and are arranged to give uniform brightness. A hole

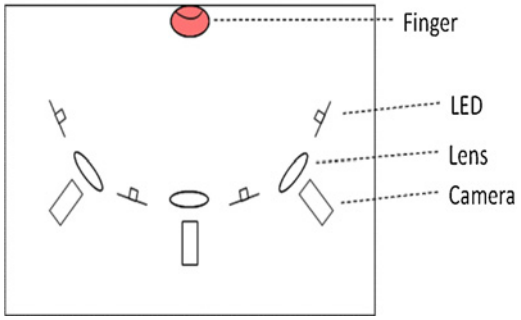

Fig. 3. Schematic diagram of the proposed touchless multiview fingerprint acquisition device.

is designed to place the finger with fixed position. The main factors which influence the captured image quality, device size, and size of overlapping region between adjacent cameras mainly include the camera and lens configuration, distance between finger and lens, color of light source, and camera numbers and arrangement. The device proposed in this paper is designed based on the camera JAI CV-A50. We next discussed the design of our device in detail as follows.

A. Lens Selection and Distance Setting

In order to capture fingerprint images with high quality and minimize the size of device, it is very important to select suitable lens and set appropriate distance between fingers and lens. Because these two factors have impact on the captured image resolution, size of the effective fingerprint area, and the height of the device. Different fingerprint features can be robustly extracted from different resolution images [15]. For traditional touch-based automated fingerprint identification systems, ∼500 and ∼800 dpi are required for minutiae and sweat pores, respectively [15]. For touchless-based systems, there is no survey showing which resolution is suitable. In [11], the resolution is larger than 500 dpi (700 dpi in center part and minimum of 500 dpi on image boarders). In [13], the resolution of captured image is ∼500 dpi. In this paper, we tried several kinds of resolutions to find an optimal one. Example fingerprint images at three kinds of resolution: ∼750, ∼500, and ∼400 dpi are shown in Fig. 4. The corresponding lens focal length and object-to-lens distance is (25 mm, 105 mm), (16 mm, 145 mm), and (12 mm, 91 mm), respectively. The image size is all restricted to 576 pixels by 768 pixels. We finally set our device lens focal length and object-to-lens distance as (12 mm, 91 mm) based on the following three reasons. Firstly, we found that ridges on fingerprint images can be extracted at all of the above-mentioned resolutions, as shown in Fig. 5. Secondly, the size of effective area is the largest one when resolution is at 400 dpi. Thirdly, the minimum object-to-lens distance is reached when resolution is ∼400 dpi.

B. Light Source Selection

Human skin has different luminous reflectance to different light sources [16]. A proper illuminator will help us to obtain touchless fingerprint images with high ridge–valley contrast.

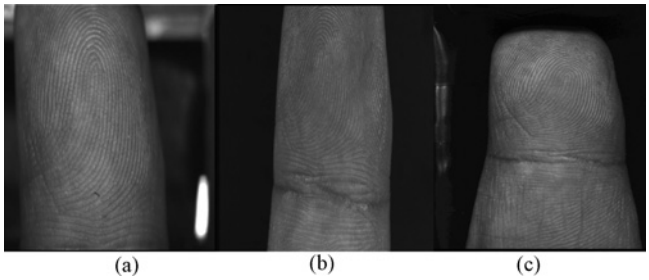

Fig. 4. Fingerprint images with respect to different resolutions. (a) ∼750 dpi. (b) ∼500 dpi. (c) ∼400 dpi.

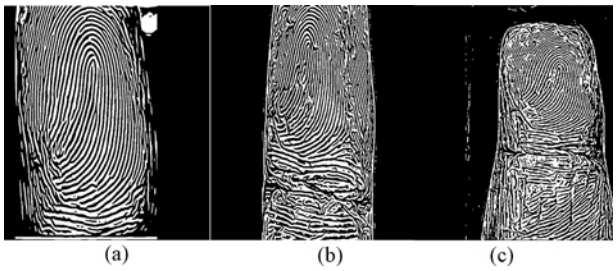

Fig. 5. Binarized fingerprint images with respect to different resolutions. (a) ∼750 dpi. (b) ∼500 dpi. (c) ∼400 dpi.

Among various kinds of light sources, blue LED and green LED are most popular ones. In [11], authors demonstrated that green light provides a higher contrast than red and blue lights. In [17], authors studied how to get high-contrast contactless fingerprint images from aspects of polarization states, illumination wavelength, detection wavelength, and illumination direction. They offered systematic evidence that blue LED is the best choice among infrared LED, red LED, green LED, and blue LED. This paper thus captured several fingerprint images using blue LED and green LED as illuminator, binarized them using the same algorithm and parameters. Fig. 6 shows an example images. We found that there is little difference between blue LED and green LED when binarizing the images by the same algorithm, as shown in Fig. 6(c) and (f). The zoomed-in segment of binarized fingerprint images using blue LED is similar with the one using green LED. Indicated by the strong evidence shown in [17], we finally chose blue LED as the light source in this paper.

C. Camera Number and Arrangement

The number of cameras directly decides the cost of the device. The smaller the number of cameras is, the cheaper the device will be. Moreover, too many views of images will aggravate the computational complexity of algorithms since there are more redundant information needs to handle with the growing of image views. Whereas, too few cameras cannot provide a sufficiently large view of the finger and result in small overlapping region between side and frontal images. Given the value of resolution r and the size of the image $w \times h$, we can easily calculate the size of measured area of the finger $W \times H$ by (1). When we set resolution as ∼400 dpi and image size as 576×768 pixels in our device, the measured area will be 36.58 mm × 48.77 mm. It is large enough to cover the size

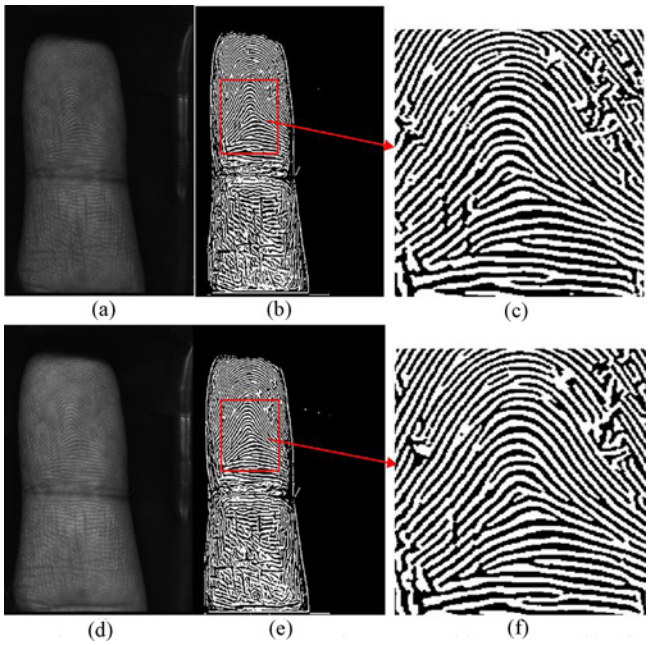

Fig. 6. Fingerprint images captured under different light sources. (a) Original image captured by using blue LED. (b) Binarized image of (a). (c) Zoomed-in segment on (b). (d) Original image captured by using green LED. (e) Binarized image of (d). (f) Zoomed-in segment on (e).

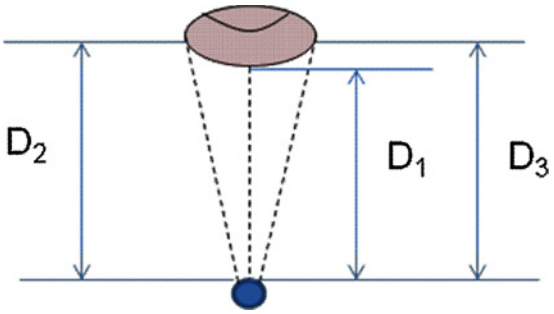

Fig. 7. Distances between lens and different parts of the finger.

of most fingers, which means that the full view of the finger can be captured by each camera in our device, as the example images shown in Fig. 8, one camera can provide the full view of the finger. However, the shape of human's fingers is curved, which leads to different distances from different parts to the lens. From Fig. 7, we can see that the distance from side parts to lens (i.e., D_2 or D_3) is larger than the distance from central part to lens (i.e., D_1). Perspective distortion is thus caused by these distance differences. As illustrated in Fig. 8, the right view of the finger disappeared when capturing images from the left side of the finger, while the left view of the finger was gone when see it from the right camera. To alleviate the perspective distortion problem in side parts of fingers, three cameras, one central camera, and two side cameras, are used in our device to capture different views of the finger, as shown in Fig. 3. In a word, we fixed our capturing device with three cameras by considering the device cost and providing a sufficiently large view of the finger simultaneously.

$$H = 25.4 \times \frac{h}{r}, W = 25.4 \times \frac{w}{r} \quad (1)$$

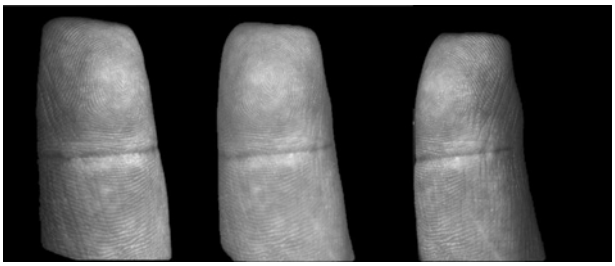

Fig. 8. Images captured by three cameras (left, frontal, and right).

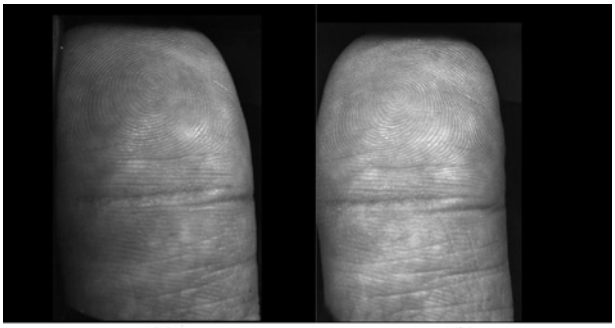

Fig. 9. Fingerprint images captured by (a) left and (b) central cameras when the angle between them is 15deg.

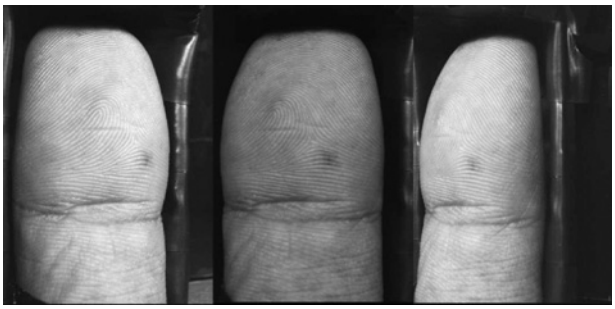

Fig. 10. Original images of a finger captured by our device (left, frontal, and right).

The placement of camera is important since it affects the size of overlapping area and the final mosaic image size. In Surround Imager™, the angle between adjacent cameras is around 45deg, while in the mirror-reflected device, the angle of mirrors is set to 15deg empirically. In our design, we tried angles of 15deg, 30deg, and 45deg. Intuitively, the smaller the angle between adjacent cameras is, the larger the overlapping region is. However, the side view of fingers cannot be captured if the angle is too small. As the example images shown in Fig. 9, when the angle is set as 15deg, the image captured by the left side camera is almost the same as the one captured by the central camera. Finally, we set the angle between central camera and side camera as roughly 30deg in our device.

To summarize, we designed the multiview touchless fingerprint capture device shown in Fig. 3 with specific parameters mentioned above. The three view images of a finger captured by our device are shown in Fig. 10.

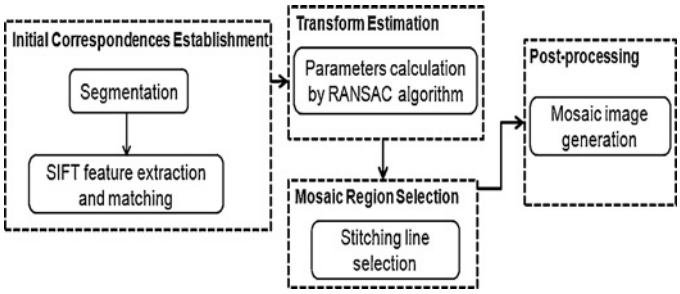

Fig. 11. Overall flow chart of the proposed fingerprint mosaicking method.

III. Fingerprint Mosaicking

As shown in Fig. 10, we can get left-side, frontal, and right-side fingerprint images at one time by our device, from which we observed that the geometrical resolution of the image decreases from the fingerprint center toward the side and the contrast of ridge and valley is not high. To overcome the drawbacks of view difference and enlarge the size of effective area, one solution is to combine these three views of images into one single image. Thus, fingerprint mosaicking is studied in this paper. Fingerprint image mosaicking is a technique for integrating different view of images into a single image with larger undistorted fingerprint area. The procedure of fingerprint image mosaicking mainly includes feature extraction, transform estimation, stitching line selection, and postprocessing. In our proposed method, we firstly preprocess the original image, extract the SIFT feature point, and establish initial correspondences by point wise matching method. Then, the parameters of thin plate spline (TPS) model are estimated for aligning the side and frontal images. After that, the stitching line is selected from the overlapping region of adjacent images. The mosaicked fingerprint image is finally generated after smoothing. The overview flow chart of the algorithm is presented in Fig. 11 and detail of the proposed approach are described as follows.

A. Initial Correspondences Establishment

To extract more accurate fingerprint features, we should segment the image into foreground and background firstly. The iterative thresholding segmentation method [27] is adopted, which can easily separate the ROI region from the background. This method selects the threshold to segment the foreground and background region in iterative fashion. In our paper, the iteration stops once the difference between the current threshold and the last one is smaller than 0.005. Finally ROI is extracted by the threshold. Fig. 12(b) and (e) show the segmentation results of Fig. 12(a) and (d). Features frequently used in fingerprint image mosaicking and matching contain minutiae, ridge map, and SIFT feature [13], [18]–[23]. In this paper, we chose to use SIFT feature in our algorithms for the following three reasons. First, due to the very low ridge–valley contrast in the fingerprint image captured by touchless imaging techniques, minutiae and ridge features are hard to correctly extract, as shown in Fig. 13. Second, because of the errors introduced in thinning ridges and localizing minutiae, minutiae- and ridge-based mosaicking cannot reach pixel-level accuracy. Thirdly, SIFT feature is robust to low image

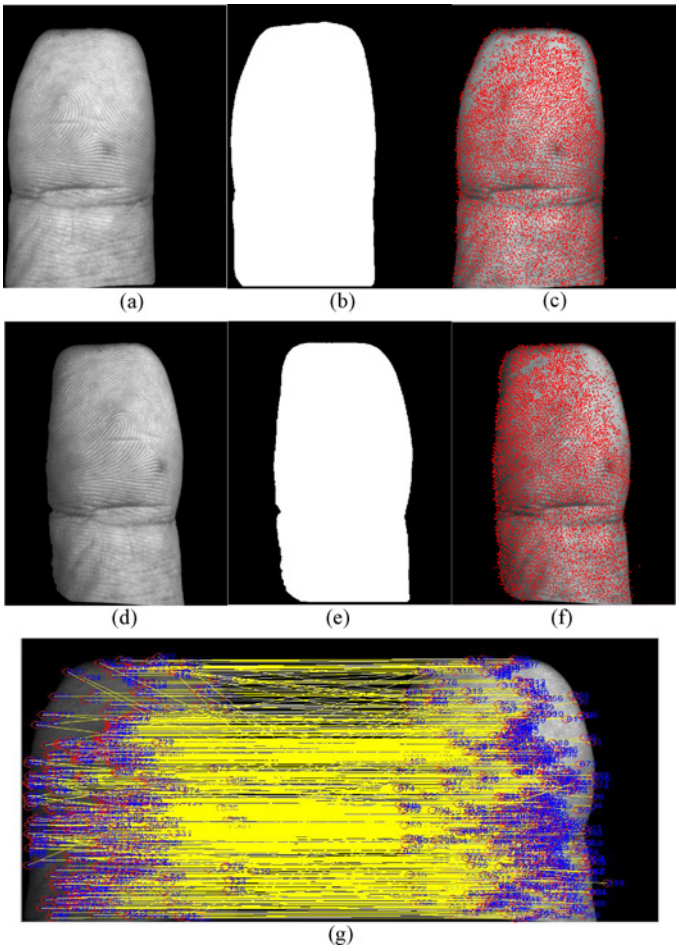

Fig. 12. Initial correspondences establishment. (a) Original frontal image. (b) Segmentation result of (a) by iterative thesholding method. (c) Extracted SIFT points from (a). (d) Original left-side image. (e) Segmentation result of (d) by iterative thesholding method. (f) Extracted SIFT points from (d). (g) Initial correspondences establishment by point wise matching.

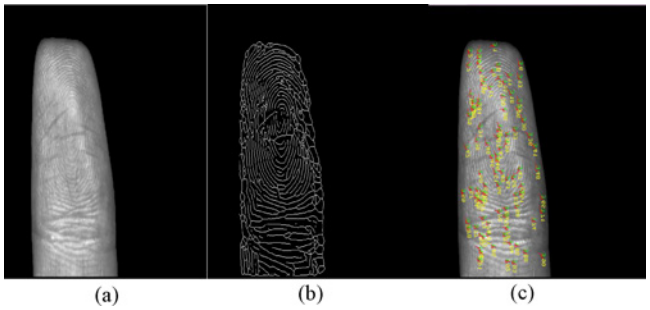

Fig. 13. Example fingerprint image with very low ridge–valley contrast. (a) Original image. (b) Ridge map. (c) Extracted minutiae.

quality and deformation variation [18]. Moreover, SIFT feature describes the local texture features exactly in pixel level and is rich in quantity [20]. SIFT [24] was popular in object recognition and image retrieval. It provides feature which is invariant to scale, rotation, and affine transforms. There are four main steps to extract SIFT features:

1) the scale-space extrema is detected from images generated by applying multiscales of difference of Gaussian (DoG) functions to the input image;

2) the accurate location of keypoint is determined according to the measurement of their stability;
3) the major orientation of each keypoint is calculated to achieve rotation-invariant keypoint descriptor (kd); and
4) SIFT feature with four properties, i.e., spatial location (x, y), scale (s), orientation (θ), and kd is finally generated. Fig. 11(c) and (f) shows the SIFT points extracted from the example fingerprint images in Figs. 11(a) and (d). There are totally 7534 and 6956 SIFT points, respectively.

After SIFT feature extraction, a point wise matching method is adopted to find correspondences between the feature sets of two images. The method is performed by comparing the associated descriptors of SIFT points. More specifically, given two SIFT feature sets P_1 and P_2 extracted from two images I_1 and I_2, we calculate the inner product between descriptor of each feature point in P_2 and descriptor of each feature point in P_1. For each feature point in P_1, we can find its top-2 closest points in P_2, whose distances to the feature point are labeled as d_1 and d_2. We then compute the ratio d_1/d_2. If the value of the ratio is sufficiently small, the point in P_1 is considered to match with the closest point in P_2. Eight hundred eleven pairs of SIFT points are matched by applying this method to Fig. 12(a) and (d), as shown in Fig. 12(g).

B. Transform Estimation

From Fig. 12(g), we can see that there are false correspondences. To estimate exact parameters of transform model between two images, we apply the classical RANSAC algorithm [25], which is insensitive to initial alignment and outliers, to calculate the optimal model parameters in an iterative fashion. The classical RANSAC algorithm mainly includes two steps. First, the minimal sample sets (MSSs) are randomly chosen from the dataset, and the parameters of the assumed global transformation model are estimated based on MSSs. Secondly, the other data in the dataset are checked to determine whether they are consistent with the model obtained in the first step. The consistent pairs form the consensus set (CS). RANSAC terminates when the probability of finding a better ranked CS drops below a certain threshold. Finally, the optimal transform model parameters and CS are both provided. It is notable that the model used in this method depends on the deformation form of the matched images. Due to the curved surface of finger and distortions introduced by cameras, we chose TPS model in the RANSAC algorithm. This model is popularly used in fingerprint domain [13], [23], [26]. Fig. 14 gives the CS when RANSAC. TPS model acted on the initial correspondences of Fig. 12(g), which demonstrated the effectiveness of the algorithm.

C. Mosaic Region Selection

Once the transform model parameters are obtained, we should determine how to stitch them to generate the final mosaic image. The approach we proposed consists of two stages. In the first phase, we extract the overlapping region of the two images. The width of the overlapping region is constrained by the maximal and minimal column coordinates given in the transformation estimation step. As shown in Fig. 15, the overlapping region on the frontal and left side images is framed by blue lines. In the second phase, we segment the overlapping region into sub-blocks with size of 21×21 pixels, and then calculate the correlation between the sub-block in left-side image and the corresponding sub-block in frontal image. The location of the stitching line is defined as the center line of the sub-block which offered the largest correlation value. The red line in Fig. 15 shows the final stitching line.

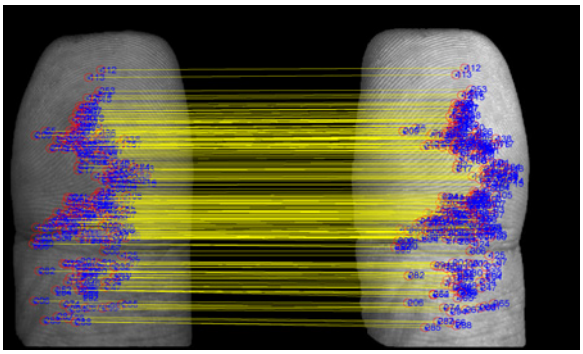

Fig. 14. CS of Fig. 12(g) obtained by RANSAC with TPS model.

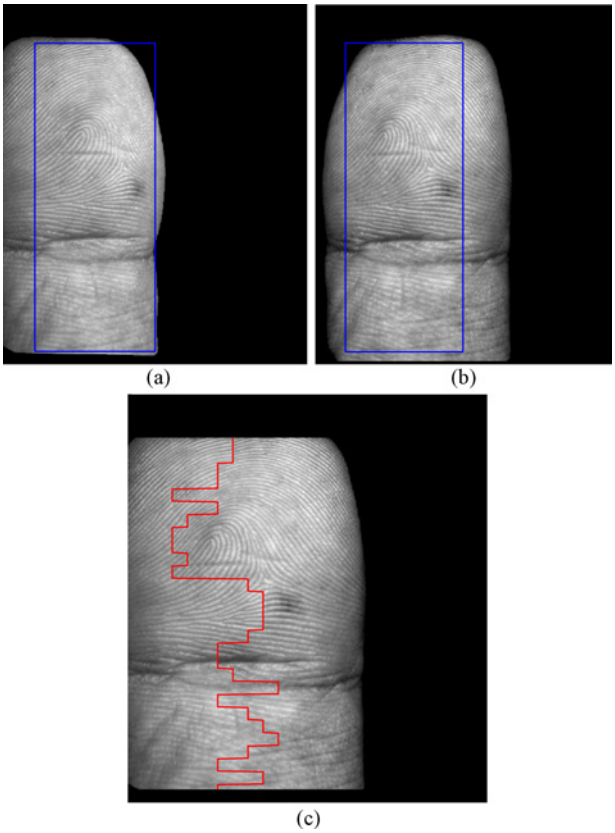

Fig. 15. Stitching line extraction. (a) Original left-side image with rectangled overlapping region. (b) Original frontal image with rectangled overlapping region. (c) Extracted stitching line.

D. Postprocess

Due to the intensity difference of images captured by separate cameras, normalization is necessary to make the

Fig. 16. Final mosaicked image for the three images in Fig. 10.

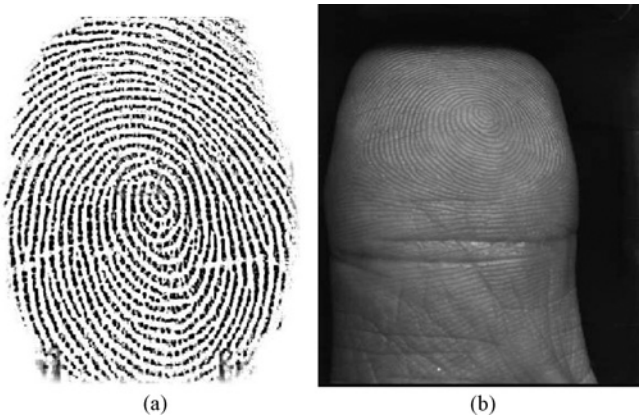

Fig. 17. Fingerprint images from the same finger. (a) Touch-based fingerprint image. (b) Frontal touchless fingerprint image.

mosaicked image smooth. Here, we used the MAX_MIN strategy to all of the images based on the intensities of their overlapping regions. Then, a Gaussian smoothing is applied to the mosaicked image to get the final result, as shown in Fig. 16.

IV. Experimental Comparison and Performance Analysis

A. Touch-Based Imaging Versus Touchless Multiview Imaging

Generally, touch-based plain fingerprint image has the advantage of high ridge–valley contrast but the disadvantage of small print size, whereas touchless multiview fingerprint imaging technique permits large print size but low image quality. To find out whether the multiview technique compensates the drawbacks of touchless imaging at certain degree, we compared recognition accuracy of touchless-based images and touch-based fingerprint images on databases of touch-based fingerprint images (collected by U.ARE.U4000) and touchless multiview fingerprint images which are collected from 215 fingers, each four examples. Fig. 17 shows examples of our collected data. We used the SIFT-based matching method

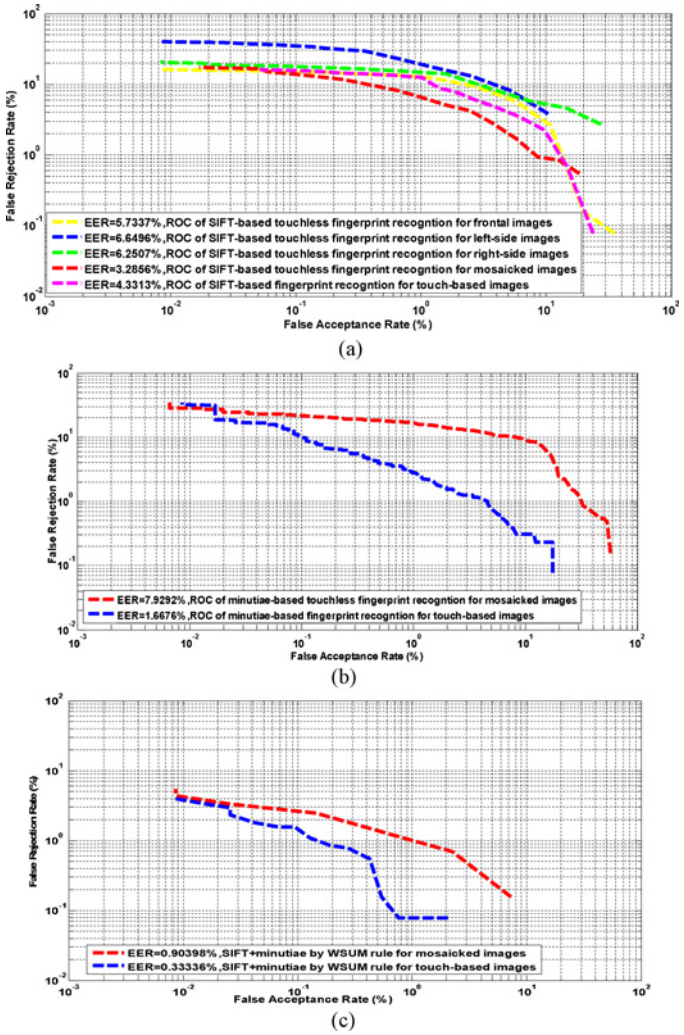

Fig. 18. Comparison of ROC curves for recognition with touchless images and touch-based fingerprint images. (a) Results with single-view touchless images, mosaicked touchless fingerprint images, and touch-based fingerprint images by using SIFT feature. (b) Results with mosaicked touchless fingerprint images and touch-based fingerprint images by using minutiae. (c) Results with mosaicked touchless fingerprint images and touch-based fingerprint images by fusing SIFT and minutiae features.

introduced in section III-A and took the size of CS as the match score. Another conventional fingerprint feature–minutia was adopted and matched by using the method introduced in [19]. The fusion results by the weighted sum (WSUM) rule [28] were also given. Fig. 18 shows the receiver operating characteristic (ROC) curves on touch-based and touchless multiview fingerprint images. As can be seen from Fig. 18(a), touch-based fingerprint recognition outperforms single-view touchless-based fingerprint recognition, whereas comparable equal error rates (EERs: ∼3.5% and ∼4%, respectively) are obtained for touch-based and mosaicked touchless fingerprint images when SIFT feature is used. When adopting minutiae for recognition, as shown in Fig. 18(b), better performance is achieved for touch-based images than for mosaicked touchless images. However, comparable performance is achieved between mosaicked touchless images and touch-base images when fusing SIFT feature and minutiae, as the results shown in Fig. 18(c) with EERs of ∼0.9% and ∼0.4%, respectively.

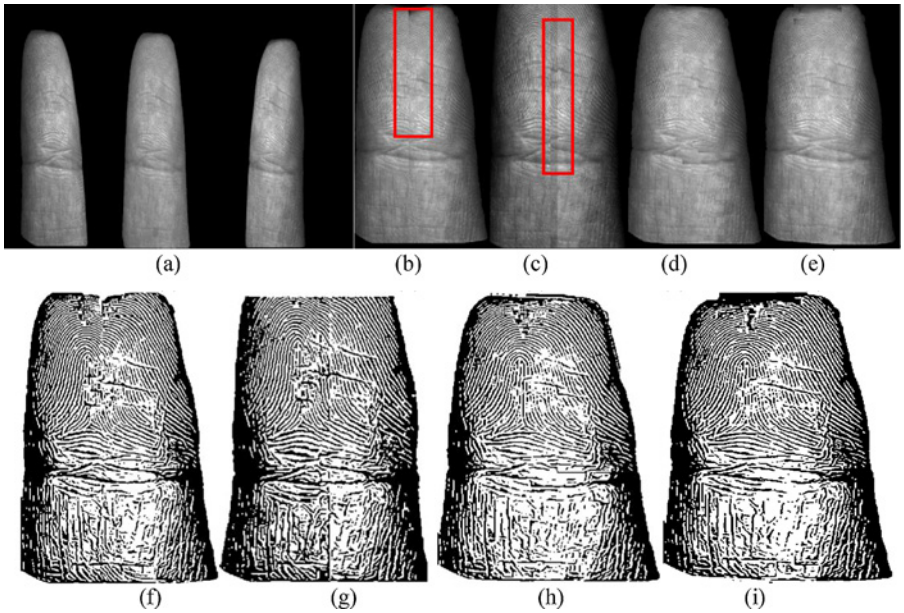

Fig. 19. Comparison of fingerprint mosaicking results. (a) Original image captured by our device. (b) Mosaicked image obtained by using the method proposed in [21]. (c) Mosaicked image obtained by using the method proposed in [22]. (d) Mosaicked image obtained by using the method proposed in [13]. (e) Mosaicked image obtained by using the method proposed in this paper. (f) Ridge map of (b). (g) Ridge map of (c). (h) Ridge map of (d). (i). Ridge map of (e).

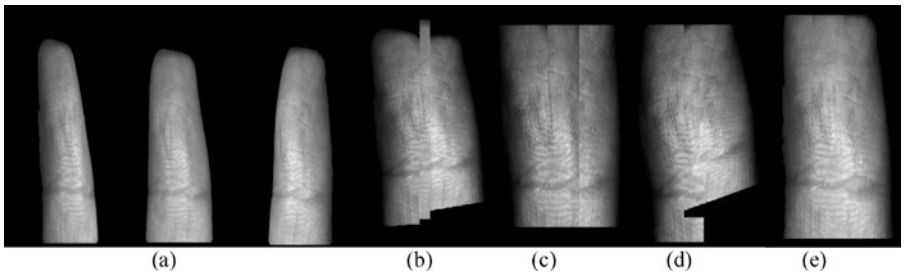

Fig. 20. Example of image mosaicking with very low ridge–valley contrast. (a) Original images captured by our device. (b) Mosaicked image obtained by using the method in [21]. (c) Mosaicked image obtained by using the method in [22]. (d) Mosaicked image obtained by using the method in [13]. (e) Mosaicked image obtained by using the method proposed in this paper.

B. Effectiveness Validation of Our Mosaic Method

To evaluate the performance of our proposed mosaic method, we firstly compared the mosaicking result got by our method with the results obtained by the approaches in [13], [21], [22]. All of the algorithms were run on our established database since the public touchless multiview fingerprint databases are unavailable. Our database contains 541 fingers from both male and female, aged 22–45. Five kinds of finger type are all included. Each finger has four samples, totally 2164 samples. Each sample consists of three views of fingerprint images. Figs. 19 and 20 show examples of mosaicked images. Comparing the mosaicked fingerprint images from them with Fig. 19(b)–(e), it can be seen that similar results are obtained by our proposed method and the one in [13], while both of them have better results in the boundary and stitching regions when compared with algorithms in [21] and [22], because i) the example images shown in Fig. 19(a) have high image quality which permits fingerprint features (minutiae and ridge features) can be correctly extracted and matched for transformation model estimation which results in similar results of the proposed method and the one in [13]; and ii) simple intensity averaging strategy is used to generate the stitching line in the algorithms of [21], [22], which leads to bad mosaicked regions (labeled by red rectangles). We can see the results more clearly from their corresponding ridge maps given in Figs 19(f)–(i). It is noted that the mosaicking methods in [13], [21], and [22] are all minutiae based. Better results can be obtained when minutiae can be correctly extracted and matched to estimate the transformation model. However, the quality of images cannot be guaranteed due to touchless imaging technique, which will lead to bad mosaicking results. Fig. 20 shows another example in which fingerprint images have very low ridge–valley contrast. Poor results are obtained by these three minutiae-based mosaicking methods but our proposed method still generates a mosaicked fingerprint image having reasonable quality.

The performance of our mosaicking algorithm was then tested and compared with the whole database. Since there are four samples for each finger, we chose the first sample of the three views (Vl_1, Vf_1, and Vr_1) to composite a mosaicked

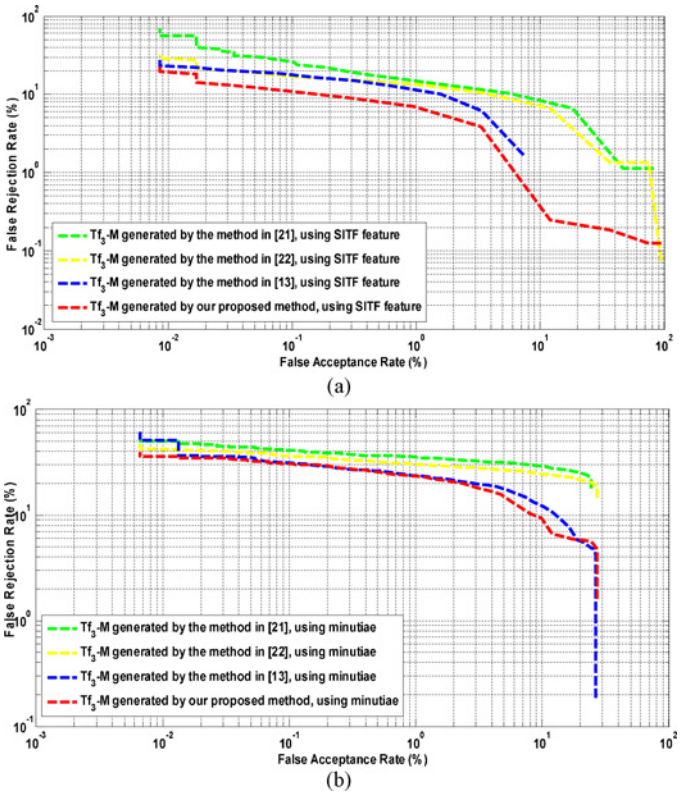

Fig. 21. ROC curves indicating mosaicking performance for different methods using (a) SIFT feature and (b) minutiae.

TABLE II
EERs Indicating Mosaicking Performance for Different Methods Using SIFT/Minutiae

Used feature EER (%) method	SIFT	Minutiae
Jain and Ross [21]	7.48	17.69
Shah *et al.* [22]	6.94	15.37
Choi *et al.* [13]	4.51	10.95
Our proposed	3.58	9.13

image (M) as the template image, and took the frontal images of the rest three samples as test images (Tf_2, Tf_3, and Tf_4). Thus, 1623 genuine pairs are generated. Fifteen thousand ten imposter pairs are selected from those image pairs created by matching M of each finger with all of the other fingers in Tf_3. The SIFT feature and minutiae are considered for matching since either of them is used in our mosaicking algorithm and methods in [13], [21], [22]. Fig. 21 shows the ROC curves of matching test images with mosaicked images generated by four different algorithms. It can be seen that the best performance is achieved when matching test image Tf_3 with mosaicked image M generated by our proposed method no matter which feature is used. EERs given in Table II further demonstrate the effectiveness of our proposed mosaicking method.

C. System Complexity Analysis

In our capturing device, we adopted three cameras made by JAI with model: CV-A50. The frame rate of each is 30 frames/s. Thus, it consumes not more than 100 ms to capture three views of fingerprint images. This time is longer than the one used up by mirror-reflected device (∼34 ms, camera frame rate: 29 frames/s), but shorter than the one expended by Surround Imager™ (120 ms), which avoided image blurring caused by finger movements. As the block diagram of our mosaicking method shown in Fig. 11, the main steps include SIFT feature extraction and matching, transform estimation, and stitching line selection. Since the computational complexity is related with the parameters of each single step, we analyzed the computational cost of our algorithm one by one. For SIFT feature extraction, the computation mainly exists in 2-D convolution between the input image and Gaussian functions with different scales, and histogram calculation when generating the kd. The corresponding complexity is $O(N^2)$ and $O(M^2)$, respectively [29], where N represents the filter size of the adopted Gaussian function and M denotes the window size when generated the descriptor. With regard to SIFT-based matching, the cost relies on the number of feature points. The complexity of $O(P \times Q)$ will be achieved, where the number of feature points in two images are denoted by P and Q. Since the RANSAC algorithm is employed to estimate the parameter of transform model, we can get the cost of $O(\hat{T}_{\text{iter}}(C_{\text{estimate}}(m) + nC_{\text{fitting}}))$ in the worst case scenario [30], where $\hat{T}_{\text{iter}} = (\log \varepsilon)/(\log(1 - q(\hat{N}_1)))$ is the iteration threshold (ε is a constant to denote the false alarm rate, $\hat{N}_1$ is the conservative estimation of the total number of inliers, and Please check the symbol here $q()$ is the probability of obtaining a MSS composed only of inliers), $C_{\text{estimate}}(m)$ denotes the cost to compute the parameters of the model starting from the MSS (whose cardinality is m), C_{fitting} represents the cost associated to compute the fitting of one single element, and n denotes the number of initial correspondences. According to the explanation of the step to select the stitching line in Section III-C, we can easily get that the complexity is $O(S^2)$, where the size of sub-block we used is S. Finally, the total computational complexity of our algorithm can be roughly expressed as $O(N^2 + M^2 + P \times Q + \hat{T}_{\text{iter}}(C_{\text{estimate}}(m) + nC_{\text{fitting}}) + S^2)$. The mosaicking method is implemented by MATLAB on Fujitsu notebook embedded Intel Core 2 Duo CPU, T9600 (2.80 GHz) processor. The execution time for the three main steps are 9.98 s, 1.34 s, 854 ms, respectively. The total time for mosaicking three views of images in our paper is about 29.65 s. But we believe this time will be largely reduced once compiling the code by C/C++ language and using the multithread processing technique.

V. Conclusion and Future Work

This paper proposed a touchless multiview fingerprint image acquisition device and associated fingerprint mosaicking method. The advantage of multiview imaging is that it obtains more fingerprint information quickly, while touchless imaging has the advantages of hygiene, avoiding fingerprint deformation, and not producing latent prints. However, touchless imaging does suffer from low ridge–valley contrast and perspective distortion between images of different views. Therefore, we designed our device by optimizing several factors which affect

the captured image quality and device size. We then proposed a mosaicking method to get expanded fingerprint images with larger effective area. When mosaicking, we used the SIFT feature which is robust to low ridge–valley contrast. Comparable recognition accuracy is achieved when comparing EERs between mosaicked images and touch-based images on established databases. Experimental results also showed that the proposed mosaicking method well works on our captured images. According to compared recognition performance of matching test images with the mosaicked images generated by different methods, we found best EERs are obtained when matching test images with the mosaicked image generated by our proposed method no matter which feature is adopted. Nonetheless, the current system still has some drawbacks which are inevitable to touchless imaging techniques. For some fingers, the image quality of the device is much lower than that of touch-based devices and some fingers are so tilted that some part of the fingerprint is out of the DOF. There are either very narrow or wide ridges in one image due to the curve surface of finger. Such low quality fingerprints and large variations of ridge frequency call for a very robust feature extraction algorithm (e.g., minutiae extraction). Considering the fact that the area of touchless fingerprints is generally larger than that of the touch-based fingerprints, we believe that the future work will enable us to extract more distinctive information from touchless fingerprints than from touch-based fingerprints. We further foresee that the current system can be improved in the following three ways: i) a more robust feature extraction algorithm is required to deal with fingerprint images of very low quality and with large variations of ridge frequency; ii) we can obtain greater accuracy by the addition of nonminutiae information (e.g., finger shape, finger crease feature, image-based features, 3-D information, and so on); and iii) we propose to explore tighter fusion schemes, such as fusion at the feature or alignment level.

ACKNOWLEDGMENT

The authors would like to thank the editor and the anonymous reviewers for their help in improving the paper.

REFERENCES

[1] S. Pankanti, S. Prabhakar, and A. Jain, "On the individuality of fingerprints," *IEEE Trans. Pattern Anal. Mach. Intell.*, vol. 24, no. 8, pp. 1010–1025, Aug. 2002.

[2] X. Xia and L. O'Gorman, "Innovations in fingerprint capture devices," *Pattern Recognit.*, vol. 36, no. 2, pp. 361–369, Feb. 2003.

[3] Y. Song, C. Lee, and J. Kim, "A new scheme for touchless fingerprint recognition system," in *Proc. Int. Symp. Intell. Signal Proces. Commun. Syst.*, Nov. 2004, pp. 524–527.

[4] Mitsubishi. *Mitsubishi Touchless Fingerprint Sensor* [Online]. Available: http://global.mitsubishielectric.com

[5] Lumidigm. *Lumidigm Multispectral Fingerprint Imaging* [Online]. Available: http://www.lumidigm.com

[6] *TST Biometrics BiRD3* [Online]. Available: http://www.tst-biometrics.com

[7] F. Chen, "3-D fingerprint and palm print data model and capture devices using multistructured lights and cameras," U.S. Patent Appl. Publ. 0120576, 2006.

[8] A. Kumar and Y. Zhou, "Contactless fingerprint identification using level zero features," in *Proc. CVPR'11 CVPR'W 2011*, Jun. 2011, pp. 114–119.

[9] A. Fatehpuria, D. Lau, and L. Hassebrook, "Acquiring a 2-D rolled equivalent fingerprint image from a non-contact 3-D finger," in *Proc. SPIE Defense Security Symp. Biometric Technol. Human Identification III*, vol. 6202, Apr. 2006, pp. 62020C-1–62020C-8.

[10] *Fingerprint Science Group: Handshot* [Online]. Available: http://privacy.cs.cmu.edu/dataprivacy/projects/handshot/index.html

[11] G. Parziale and E. Diaz-Santana, "The surround imager: A multicamera touchless device to acquire 3-D rolled-equivalent fingerprints," in *Proc. Int. Conf. Biometrics (ICB)*, vol. 3832, 2006, pp. 244–250.

[12] *TBS Touchless Fingerprint Imaging: 3-D-Enroll, 3-D-Terminal* [Online]. Available: http://www.tbsinc.com

[13] H. Choi, K. Choi, and J. Kim, "Mosaicing touchless and mirror-reflected fingerprint images," *IEEE Trans. Inform. Forensics Security*, vol. 5, no. 1, pp. 52–61, Mar. 2010.

[14] Y. Chen, "Extended feature set and touchless imaging for fingerprint matching," Ph.D. dissertation, Michigan State Univ., East Lansing, MI, USA, 2009.

[15] D. Zhang, F. Liu, Q. Zhao, G. Lu, and N. Luo, "Selecting a reference high resolution for fingerprint recognition using minutiae and pores," *IEEE Trans. Instrum. Meas.*, vol. 60, no. 3, pp. 863–871, Mar. 2011.

[16] A. Elli, "Understanding the color of human skin," in *Proc. 6th SPIE Conf. Human Vision Electron. Imag. SPIE*, vol. 4299, 2001, pp. 243–251.

[17] L. Wang, R. El-Maksoud, J. Sasian, and V. Valencia, "Illumination scheme for high-contrast, contactless fingerprint images," *Proc. SPIE*, vol. 7429, pp. 742911-1–742911-7, 2009.

[18] U. Park, S. Pankanti, and A. Jain, "Fingerprint verification using SIFT features," *Proc. SPIE*, vol. 6944, pp. 69440K–69440K-9, 2008.

[19] J. Feng, "Combining minutiae descriptors for fingerprint matching," *Pattern Recognit.*, vol. 41, no. 1, pp. 342–352, Jan. 2008.

[20] S. Malathi and C. Meena, "Partial fingerprint matching based on SIFT features," *Int. J. Computer Sci. Eng.*, vol. 2, no. 4, pp. 1411–1414, 2010.

[21] A. Jain and A. Ross, "Fingerprint mosaicking," in *Proc. IEEE Int. Conf. Acoust. Speech Signal Proces. (ICASSP)*, vol. 4, May 2002, pp. IV-4064–IV-4067.

[22] S. Shah, A. Ross, J. Shah, and S. Crihalmeanu, "Fingerprint mosaicking using thin plate splines," in *Proc. Biometric Consortium Conf.*, Sep. 2005.

[23] K. Choi, H. Choi, S. Lee, and J. Kim, "Fingerprint image mosaicking by recursive ridge mapping," *IEEE Trans. Syst., Man, Cybern., B*, vol. 37, no. 5, pp. 1191–1203, Oct. 2007.

[24] D. Lowe, "Distinctive image features from scale-invariant keypoints," *Int. J. Computer Vision*, vol. 60, no. 2, pp. 91–110, Nov. 2004.

[25] M. Fishler and R. Bolles, "Random sample consensus: A paradigm for model fitting with applications to image analysis and automated cartography," *Commun. ACM*, vol. 24, no. 6, pp. 381–395, Jun. 1981.

[26] A. Ross, S. Dass, and A. Jain, "A deformable model for fingerprint matching," *Pattern Recognit.*, vol. 38, no. 1, pp. 95–103, Jan. 2005.

[27] J. Kittler, J. Lllingworth, J. Foglein, and K. Paler, "An automatic thresholding algorithm and its performance," in *Proc. 7th Int. Conf. Pattern Recognit.,* vol. 1, 1984, pp. 287–289.

[28] Q. Zhao, L. Zhang, D. Zhang, and N. Luo, "Direct pore matching for fingerprint recognition," in *Proc. ICB*, vol. 5558, Jun. 2009, pp. 597–606.

[29] M. Grabner, H. Grabner, and H. Bischof, "Fast approximated SIFT," in *Proc. ACCV*, 2006, pp. 918–927.

[30] M. Zuliani. (2008). *RANSAC for Dummies* [Online]. Available: http://www.vision.ece.ucsb.edu/∼zuliani/Research/RANSAC/docs/RANSAC4Dummies.pdf

Feng Liu received the B.S. and M.S. degrees both from the Department of Electrical and Engineering, Xidian University, Xi'an, Shaanxi, China, in 2006 and 2009, respectively. She is currently pursuing the Ph.D. degree in computer science at the Department of Computing, Hong Kong Polytechnic University, Kowloon, Hong Kong.

Her current research interests include pattern recognition and image processing, especially with a focus on their applications to fingerprints.

David Zhang graduated in computer science from Peking University, Beijing, China. He received the M.Sc. degree in computer science and the Ph.D. degree from the Harbin Institute of Technology (HIT), Harbin, China, in 1982 and 1985, respectively, and the second Ph.D. degree in electrical and computer engineering from the University of Waterloo, Waterloo, ON, Canada, in 1994.

From 1986 to 1988, he was a Post-Doctoral Fellow at Tsinghai University, Beijing, and then an Associate Professor at Academia Sonica, Beijing. He is currently the Head of the Department of Computing, and a Chair Professor at Hong Kong Polytechnic University, where he is the Foundation Director of the Biometrics Technology Centre (UGC/CRC) supported by the Hong Kong SAR Government in 1998. He also serves as a Visiting Chair Professor at Tsinghua University and an Adjunct Professor at Shanghai Jiao Tong University, Peking University, Harbin Institute of Technology, and the University of Waterloo. He is an author of more than ten books and 250 journal papers.

Prof. Zhang is a Croucher Senior Research Fellow, Distinguished Speaker of the IEEE COMPUTER SOCIETY, and a fellow of both IEEE and IAPR. He is the Founder and the Editor-in-Chief of the *International Journal of Image and Graphics (IJIG)*, a Book Editor of Springer *International Series on Biometrics (KISB)*, an Organizer of *The First International Conference on Biometrics Authentication*, an Associate Editor of more than ten international journals, including the IEEE TRANSACTIONS AND PATTERN RECOGNITION, the Technical Committee Chair of IEEE CIS

Changjiang Song received the B.S. degree in industrial engineering from Jilin University, Changchun, China, in 2005, and the master's degree in control engineering from the Aerospace Faculty, Harbin Institute of Technology, Harbin, China, in 2012. In 2011, he went to Hong Kong Polytechnic University, Hung Hom, Hong Kong, for exchange learning.

He is currently a Research Associate at the Heilongjiang Academy of Sciences, Institute of Automation. His current research interests include computer vision, especially in phase shift of projection measurement, binocular stereo vision measurement, camera demarcation technology and realization, and related techniques of image processing and pattern recognition.

Guangming Lu received the Graduate degree in electrical engineering, the master's degree in control theory and control engineering, and the Ph.D. degree in computer science and engineering from the Harbin Institute of Technology (HIT), Harbin, China, in 1998, 2000, and 2005, respectively.

From 2005 to 2007, he was a Post-Doctoral Fellow at Tsinghua University, Beijing, China. He is currently an Associate Professor at the Biocomputing Research Center, Shenzhen Graduate School, HIT. His current research interests include pattern recognition, image processing, and automated biometric technologies and applications.